Research Square

Preprints are preliminary reports that have not undergone peer review.
They should not be considered conclusive, used to inform clinical practice,
or referenced by the media as validated information.

Exploration of Anti-inflammatory Mechanism of Forsythiaside A and Forsythiaside B in CuSO4-Induced Inflammation in Zebrafish by Metabolomic and Proteomic Analyses

Lihong Gong
Chengdu University of Traditional Chinese Medicine
Linyuan Yu
Chengdu University of Traditional Chinese Medicine
Xiaohong Gong
Chengdu University of Traditional Chinese Medicine
Cheng Wang
Chengdu University of Traditional Chinese Medicine
Naihua Hu
Chengdu University of Traditional Chinese Medicine
Xuyang Dai
Chengdu University of Traditional Chinese Medicine
Yunxia Li (lyxcdutcm@126.com)
Chengdu University of Traditional Chinese Medicine https://orcid.org/0000-0003-1307-4335

Research

Keywords: Forsythiaside A, Forsythiaside B, zebrafish, inflammation, Metabolomics, Proteomics

Posted Date: December 30th, 2019

DOI: https://doi.org/10.21203/rs.2.19758/v1

License: This work is licensed under a Creative Commons Attribution 4.0 International License. Read Full License

Version of Record: A version of this preprint was published at Journal of Neuroinflammation on June 3rd, 2020. See the published version at https://doi.org/10.1186/s12974-020-01855-9.

Abstract

Background: Inflammation is a general pathological phenomenon that operates during severe disturbance of homeostasis. Forsythiaside A (FA) and Forsythiaside B (FB) are isolated from air-dried fruits of Forsythia suspensa, which show a significant effect against inflammation. However, the anti-inflammatory effect and therapeutic mechanism have not yet been clarified in zebrafish.

Methods: In this study, the anti-inflammatory effects of FA and FB were investigated in $CuSO_4$-induced zebrafish model. Intracellular ROS and NO generation in zebrafish were performed using fluorescent probe dyes. Metabolomics and proteomics using liquid chromatography mass spectrometry were carried out to identify the expression of metabolites and proteins associated with chemically induced inflammation in zebrafish larvae. Quantitative PCR was performed to detect the progressive changes in the genes.

Results: FA and FB inhibited neutrophils migration to the damaged neuromasts and remarkably reduced $CuSO_4$-induced ROS and NO generation in zebrafish. Metabolomics analyses indicated that the Nicotinate and nicotinamide metabolism, Amino sugar and nucleotide sugar metabolism, Pyrimidine metabolism and Purine metabolism were mainly involved. The proteomic analyses identified 146 differentially expressed proteins, among which, the expression of collagen (col2a1b, col9a2, col9a1b), nme3, wdr3, mrps7, srpx, gch2, ptpn11a, rcvrn2, nit2, scaf4a and zgc:162509 were all reversed both in FA and FB groups. FA and FB could reverse the abnormal expression of these metabolites and proteins to alleviate chemical damage to the neuromasts in the lateral line of zebrafish.

Conclusions: FA and FB possess remarkable anti-inflammatory effect and could be used to protect chemically induced neuromasts damage in zebrafish larvae.

1. Background

Inflammatory response is a key component in normal homeostasis that protects the body from irritation and restores damaged tissue structure and function. Generally, inflammatory reactions are beneficial to the body. However, excessive and uncontrolled inflammation can cause chronic diseases as bowel inflammation, Alzheimer's and cancer [1, 2] etc. During this process, the over-activation of macrophages and neutrophils can induce the secretion of IL-6, TNF-α and IL-1β, which are significant mediators participating in inflammation [3].

Forsythiae fructus, also named lianqiao in China, is the dried fruit of Forsythia suspensa. As a heat-clearing and detoxifying traditional Chinese medicine, Forsythiae fructus has been used for various infectious diseases, such as acute nephritis and ulcers [4]. Up to now, more than three hundred chemical constituents have been isolated from Forsythia suspensa. Forsythiaside, the major bioactive components extracted from Forsythiae fructus, including Forsythiaside A-K. Among which, FA (Fig. 1A) and FB (Fig. 1B) are the major bioactive components extracted from Forsythiae fructus, which share the same maternal nucleus, have been reported to possess anti-inflammatory and anti-bacterial effects [5, 6]. However, few studies have been carried out to study anti-inflammatory effects and mechanisms of FA and FB based on the same inflammatory model. Whether they share consistent mechanism of action or the mechanism of action is related to the structure of maternal nucleus is worth of further study.

The vertebrate model organism of zebrafish (Danio rerio) has been widely used, of which morphological and physiological functions are similar to humans. The obvious transparency of zebrafish embryos and availability of zebrafish transgenic line make it possible to monitor inflammatory processes and observe cells behavior in vivo [7]. Researches have shown that the zebrafish immune system has significant similarities with humans, and almost all human immune system cells have counterparts in zebrafish [8]. Copper sulfate can cause chemical damage to the neuromasts in the lateral line system of zebrafish, which are composed of mechanosensory hair cells and can be damaged by physical or chemical stimulation. Unfortunately, the role of FA and FB in the zebrafish immune system and their molecular mechanisms still remain to be further studied.

Presently, we explored the anti-inflammatory mechanism of FA and FB via an untargeted metabolic and proteomics profiling of the zebrafish based on LC-MS. The results showed that the expression of a series of metabolites and proteins were altered during the inflammatory process. Therefore, we proposed a potential mechanism to explain the inflammatory neuromasts behavior of zebrafish induced by copper sulfate and highlight the therapeutic effects of FA and FB for inflammation.

2. Methods

2.1 Materials

FA (MUST-18010303) and FB (MUST-18081202) were purchased from Chengdu MUST Bio-technology Co., Ltd (Chengdu, China). Acetonitrile, Methanol and Formic acid of HPLC grade were collected from Merck Chemicals (Shanghai, China), Wokai Chemical Technology Co., Ltd. (Shanghai, China) and TCI Chemical Industry Development Co., Ltd. (Shanghai, China), respectively. DAF-FMDA and DCF-DA were purchased from Yeasen (Shanghai, China). Trizol reagents were purchased from Ambion Life Technologies (Carlsbad, CA, USA). 5 × All-In-one MasterMix and Eva Green 2 × qRT-PCR MasterMix-Low RoX were purchased from Applied Biological Materials Inc (Richomnd, BC, Canada). PCR primer sequences were synthesized in TSINGKE Biological Technology (Chengdu, China). Other chemicals and reagents were obtained from Kelong Chemical Reagent Factory (Chengdu, China).

2.2 Zebrafish

Zebrafish (Danio rerio) of wild-type AB and transgenic (mpx:EGFP) were purchased from China Zebrafish Resource Center (Wuhan, China) and raised in following conditions: 28.5 ± 1.0℃ of water temperature, 6.9–7.5 of pH, dark/light cycle of 10/14 h. The male and female (1:1) were placed in a sphwning tank the day before. In general, zebrafish naturally propagated embryos within 30 minutes after turning on the lights in the morning [9]. Zebrafish embryos were collected and raised in the above conditions till drug administration.

2.3 Drug administration and in vivo neutrophil recruitment assay

All experiments were performed on 3-day post-fertilization (dpf) zebrafish larvae in the present study. Transgenic (mpx:EGFP) zebrafish were randomly transferred to the twelve-well plate (15 larvae per well) and assigned to 8 groups for neutrophil recruitment investigation: larvae incubated in zebrafish embryonic medium, a control group; larvae exposed to 10 μmol•L^{-1} $CuSO_4$ for 40 min only, a model group; FA treatment

groups of larvae pre-incubated with FA (120, 60, 30 μmol•L^{-1}) only for 1 hour followed by 40 min incubation with a mixture of 10 μmol•L^{-1} $CuSO_4$ and different concentrations of FA (120, 60, 30 μmol•L^{-1}), respectively; FB treatment groups of larvae pre-incubated with FB (150, 75, 37.5 μmol•L^{-1}) only for 1 hour followed by 40 min incubation with a mixture of 10 μmol•L^{-1} $CuSO_4$ and different concentrations of FB (150, 75, 37.5 μmol•L^{-1}), respectively. All drugs were diluted in 1 × E3 medium (5.00 mmol•L^{-1} NaCl, 0.44 mmol•L^{-1} $CaCl_2$, 0.33 mmol•L^{-1} $MgSO_4$ and 0.17 mmol•L^{-1} KCl). After the treatments, tricaine solution (Sigma, Shanghai, China) were performed on zebrafish larvae for anesthetization. Then zebrafish were observed under Leica M165Fic fluorescence microscope and photographed. The recruitment number of neutrophils to neuromasts in zebrafish was counted by image pro plus software.

2.4 Measurement of intracellular production of ROS and NO in zebrafish

Presently, fluorescent probe dyes of DCF-DA and DAF-FMDA were used to investigate the intracellular ROS and NO accumulation in $CuSO_4$-induced zebrafish, respectively [10]. After the treatments, zebrafish were moved to twelve-well plates (15 larvae per well) and treated with DCF-DA (0.05 μmol•L^{-1}) and DAF-FMDA (5 μmol•L^{-1}) solution, respectively. It was then incubated for 1 h darkness treatment. Zebrafish were washed with fresh medium after incubation and anesthetized with tricaine. The accumulation of ROS and NO in zebrafish were photographed under a Leica M165Fic fluorescence microscope. Finally, image pro plus software was used to quantitatively analyze the fluorescence intensity of individual zebrafish larvae.

2.5 Metabolomics: sample processing and detection for metabolites

100 mg samples (about 250 zebrafish larvae) of 10 biological replicates of zebrafish from control, model, FA (120 μmol•L^{-1}) and FB (150 μmol•L^{-1}) groups were transferred to 2 mL centrifuge tubes, respectively (insufficient sample size is reduced to an equal scale). 1000 μL of 80% methanol and steel balls were added to tubes. Samples were grinded for 1 min in a tissue grinding device at 70 Hz. Then tubes were put in the ultrasonic machine for 30 min. Tubes were stewed 30 min on ice, centrifuged for 10 min (14, 000 rpm, 4℃) and supernatants were moved to a new tube. After vacuum centrifugation concentrating, samples were dissolved by 400 μL 2-chlorobenzalanine (4 ppm) methanol aqueous solution (1:1,4℃), and were prepared for LC-MS detection following filtration (0.22 μm). Quality control samples were prepared by mixing 20 μL of each sample. LC-MS detection was performed for the remaining samples.

Chromatographic separation was performed on the Thermo Ultimate 3000 system, equipped with a Waters column (1.8 um, 150 × 2.1 mm) of 40℃. 8℃ was set as the autosampler temperature. 0.1% formic acid in water (C) and 0.1% formic acid in acetonitrile (D) or 5 mmol•L^{-1} ammonium formate in water (A), acetonitrile (B) were performed for gradient elution at 0.25 ml•min^{-1}. Each sample of 2 μL was injected after equilibrated. The solvent B (v/v) increases as follows: 0–1 min, 2% B/D; 1–9 min, 2%-50% B/D; 9–12 min, 50%-98% B/D; 12-13.5 min, 98% B/D; 13.5–14 min, 98%-2% B/D; 14–20 min, 2% D-positive model (14–17 min, 2% B-negative model).

The ESI-MSn experiments in positive and negative ion mode were performed on Thermo Q Exactive Focus spectrometer with sparge voltages of 3.8 KV and − 2.5 KV, respectively. Sheath gas was set at 45 arbitrary units, while auxiliary gas was set at 15, with 325°C of capillary temperature. The Orbitrap analyzer performs a full scan with a mass range of m/z 81-1000 and a mass resolution of 70, 000. MS/MS experiments were data-dependently acquired by HCD scanning. The standard collision energy was 30 ev. In order to remove some unnecessary information in MS/MS spectrum, dynamic exclusion is implemented.

2.6 Statistical rationale

Data of UPLC-MS/MS was displayed in mzXML format via Proteowizard software (v3.0.8789). Data pre-processing was performed by XCMS program of R (v3.3.2). Parameters were mainly set as follows: bw = 2, ppm = 15, mzwid = 0.015, peak width = c (5, 30), mzdiff = 0.01, method = cent wave. The area of metabolite peaks in each sample was normalized by the summation method applied in metaboanalyst. Multivariate analysis of metabolites including standard peak areas and retention time were performed using R language tools package. Data were processed by autoscaling, mean-centering and scaled to unit variance, followed by multivariate analysis. Orthogonal projections to latent structures discriminant analysis (OPLS-DA) and Student's t-test were used to filter metabolites significantly contributed to group discrimination by VIP values. Differential metabolites with VIP ≥ 1 were checked by S-Plot and were selected if $P \leq 0.05$. The biomarker formulation was generated and queried of accurate molecular weights with mass errors less than 30 ppm. The fracture patterns of potential biomarkers were analyzed and identification of these biomarkers were performed by other databases, such as Human Metabolome Database (HMDB) (http://www. hmdb. ca) and METLIN (http://metlin.scripps. edu/). KEGG database was used to plot metabolomics pathway network diagram. Pathway enrichment analysis by metaboanalyst was performed to analyze metabolomics pathway of identified metabolites in the current study.

2.7 Proteomics: protein extraction and digestion

Proteins were extracted from 3 biological replicates of zebrafish from control, model, FA (120 μmol•L^{-1}) and FB (150 μmol•L^{-1}) groups as previously described [11]. Briefly, 500 μL of Lysis Buffer (2% sodium deoxycholate, 50 mM ammonium bicarbonate, 75 mM sodium chloride) was added to samples (about 250 zebrafish larvae per sample), which were then ground. After placing on ice for 10 min at 2 s on and 4 s off at 15% power (Scientz-JY92, Ningbo xinzhi biotechnology co., LTD), the ground material was centrifuged for 10 min (10, 000 g, 4 °C). Proteins was extracted by precipitation of acetone at -20°C as previously described [12]. Air-dried precipitated proteins were then resuspended with Lysis Buffer. The concentration of protein was detected using BCA assay as the standard. The resulting supernatants were incubated with final DTT concentration to10 mmol•L^{-1} at 56 °C for 1 h, followed by alkylation with 55 mmol•L^{-1} iodoacetamide for 45 min darkness treatment at a room temperature. The protein solution (100 μg) was digested by Trypsin Gold at 37 °C overnight (40:1, protein: trypsin). A Strata X C18 column was used for peptides desalination and then vacuum-dried in accordance with the manufacturer's instructions.

2.8 TMT labeling and fractionation

The peptides were labeled using TMT six plex Isobaric Label Reagent Set (Thermo Scientific, 90061) in accordance with manufacturer's instructions. Samples of control and model groups were labeled with TMT tags 126 and 127, while samples of FA and FB groups were labeled with tags 128 and 129. The labeled

peptides were separated using Shimadzu LC-20AB HPLC Pump system (Shimadzu, Kyoto, Japan) equipped with a high-pH RP column. Then labeled peptides were firstly regenerated with buffer A (5% ACN and 95% H_2O, pH was adjusted to 9.8 with ammonia 2.7) and loaded on the column that contains 5 μm particles (Phenomenex, CA, USA). Peptides were separated at 1 ml•min^{-1} in the following conditions: 5% buffer B (5% H_2O and 95% ACN, pH was adjusted to 9.8 with ammonia),10 min; 5–35% buffer B, 40 min; 35–95% buffer B, 1 min. Then the system was maintained for 3 min in 95% buffer B and buffer B was reduced to 5% within 1 min and equilibrated for 10 min in this condition. The peptides were collected at absorbance of 214 nm every 1 min and pooled as 20 fractions. Vacuum centrifugation was carried out for concentration.

2.9 LC-MS/MS Analysis

The fractions were resuspended in Buffer A (2% acetonitrile and 0.1% formic acid). Then it was centrifuged for 10 min (20, 000 × g). Supernatants were loaded to the C18 trap column on a LC-20 AD nano-HPLC instrument. An internally packed analytical C18 column were used to elute and separate the peptides. The elution procedure was performed at 600 nl·min^{-1} under the following conditions: 8–35% buffer B, 35 min; 60% buffer B, 5 min; 80% buffer B, 5 min; 5% buffer B, 0.1 min. The equilibration time is 10 min. The eluted peptide was subjected to nano-electrospray ionization, and then analyzed by MS/MS (Orbitrap Fusion Lumos mass spectrometer, CA, USA) and a nano HPLC system. The mass spectrometry analyses were performed in data-dependent mode of 350–1800 m/z scan range. The survey scans were obtained at 120, 000 mass resolution of 400 m/z via Orbitrap analyzer. Dynamic exclusion parameters mainly include count of 2 and time of 30 s.

2.10 Identification and quantification of proteins

Proteome Discoverer software v2.1 (Thermo Fisher Scientific, Massachusetts, USA) was applied to process and quantify raw data files. Protein search was performed in the RefSeq Human protein database (24078 sequence, released in 2017) based on SEQUEST algorithm. Parameters were set as follows: fixed modification, involving cysteine carbamidomethylation; modification of N terminus and K of TMT six-plus. And methionine oxidation was applied as variable modification. The enzyme is set as trypsin, allowing 2 missing cleavages. The verification and identification were performed by the Percolator software. The protein and peptide profile matching false discovery rate (FDR) was set to 0.01 [13]. Total protein intensity is generated by summing all reported ion intensities of unique peptides that match to each respective protein. Correction of Bias and Background were performed by checking protein quantification and normalization. Proteins containing at least two unique peptides were further quantified. Accordingly, differential expressed proteins were identified with a p-value < 0.05 and fold change > 1.2.

2.11 Interactive network construction of metabolites and proteins

For pathway and network analyses, the correlation coefficient and p-value of the differentially expressed metabolites and proteins (with NCBI IDs) were calculated by R language. The metabolites and proteins with p-value < 0.05 and absolute correlation coefficient > 0.9 were screened out, and further imported into Cytoscape software to generate the final association analysis network diagram.

2.12 Quantitative real-time PCR analysis

PCR reactions were performed to analyze the mRNA expression of MRPS7, WDR3, NME3, Collagen, inflammation mediators and genes involved in NF-κB, MAPK and JAK-STAT signaling pathways. In brief, zebrafish were washed three times with RNase-free water, which were then homogenized with Trizol reagent. Homogenized tissues were extracted by chloroform and centrifugated for 15 min (12, 000 × g, 4 °C). The supernatant was transferred to a new tube and isopropyl alcohol with equal volume was added for RNA precipitation. After being centrifuged for 10 min (12, 000 × g, 4°C), 75% ethanol was used to wash the pellet. Then it was dried and dissolved in 50 μl RNase-free water. The OD260/280 value was measured for RNA purity detection. The reaction procedures were set as follows: 95 °C for 10 min, 95 °C for 15 s, 60 °C for 30 s (40 cycles). The relative mRNA expressions were shown by calculating values of $2^{-\Delta\Delta CT}$. Primers of all genes for amplification were designed by Primer-BLAST (NCBI) as listed in Table S1.

2.13 Data and statistical analysis

Zebrafish larval were assigned to each treatment group randomly and pharmacodynamic experiments were repeated three times. SPSS 25.0 software and GraphPad Prism 6.0 software were performed for statistical analyses. All data points were included from the analysis in the present study. The n value in all experiments was adopted based on our previous experiment as shown in the figure legend. All data were shown as mean ± S.D. Statistical comparisons were performed using one-way ANOVA, and $P < 0.05$ were assumed for statistical significance indication.

3. Results

3.1 Inhibitory effects of FA and FB in $CuSO_4$-induced inflammation

The primary lateral line system of zebrafish is well established within 3 days after fertilization. Previous studies have reported that the addition of copper can swiftly destroy the hair cells of neuromasts in zebrafish lateral line through oxidation and cell death [14]. The zebrafish larvae of each treatment group were observed by the fluorescence microscope and the number of fluorescent cells in region of about ten cell diameters within the horizontal muscle of zebrafish was counted (Figure 2A). In the control group, most of the neutrophils are in the blood island and hematopoietic tissues, areas where most leukocytes are distributed in this development stage. In contrast, zebrafish exposed to 10 μmol•L^{-1} $CuSO_4$ for 40 min formed a typical neutrophil cluster in horizontal muscles, which indicates that neutrophils actively migrated to the neuromasts lateral line under the induction of copper sulfate. In contrast to copper exposure, co-treatment with FA and FB inhibited neutrophils migration and decreased the assembled number of neutrophils (Figure 2B). These results indicated that FA or FB treatment can dose dependently inhibit neutrophils recruitment to the neuromasts of zebrafish lateral line (Figure 2C).

3.2 Inhibitory effect of FA and FB against $CuSO_4$-induced intracellular ROS and NO generation in zebrafish larvae

The overproduction of ROS by polymorphonuclear neutrophils at the inflammation site can cause endothelial dysfunction and tissue damage [15]. Therefore, DCF-DA was used to determine ROS generation in $CuSO_4$-induced zebrafish inflammation model. Figure 3A exhibits a representative image of intracellular ROS production and inhibitory effects of FA and FB on ROS accumulation in a $CuSO_4$-induced zebrafish model. The control group, which was not treated with $CuSO_4$ or FA and FB, exhibited a clear and weaker fluorescent image. However, the model group, which was exposed to $CuSO_4$, showed a bright and strong fluorescent image. Thus, addition of $CuSO_4$ in water can lead to intracellular ROS generation in zebrafish. However, FA and FB treatment dose-dependently decreased intracellular ROS accumulation in zebrafish (Figure 3B).

Besides, NO is also a common conduction molecule and plays an important role in the initiation and development of inflammation [16]. Hence, the fluorescent robe dye DAF-FMDA was performed to evaluate the inhibition of FA and FB in $CuSO_4$-induced intracellular NO production in zebrafish. As a result, zebrafish exposed to $CuSO_4$ only showed an excessive generation of NO (Figure 3C). However, zebrafish pre-treated with FA or FB showed a significant decrease of NO accumulation in a dose-dependent manner (Figure 3D). These evidences indicated that FA and FB relieved $CuSO_4$-induced zebrafish inflammatory process via inhibiting generation of intracellular ROS and NO.

3.3 Multivariate data analysis of UPLC-MS/MS data

UPLC-MS/MS was used to analyze all zebrafish samples in positive and negative ion mode, respectively. Representative base peak chromatograms (BPC) of 4 groups of zebrafish samples were obtained under optimal conditions (Figure 4A, 4B). 15489 variables (ESI+) and 26308 variables (ESI-) could simultaneously be detected in 20 min.

Multivariate analysis suggesting good separations among the control, model, FA and FB treatment groups. A principal component analysis (PCA) model of metabolomics of each group, and the profiles of different groups showed a tendency towards separation (Figure 4C, 4D). As a model for supervised analysis, partial least squares-discriminant analysis (PLS-DA) was performed and could further distinguish the differences in metabolites among four groups. The scores plot of PLS-DA indicated that the four groups were clearly distinguished (Figure 4E, 4F). It was found that the control group and model group were obviously separated both in positive mode and negative mode, indicating a $CuSO_4$-induced zebrafish acute inflammation model was successfully established. FA and FB groups were closer to the control group, which highlighted the anti-inflammation effects of drugs.

3.4 Identification and analysis of metabolites

Potential biomarkers were first selected based on VIP values and then analyzed by Student's t test. Variables with statistical significance ($P \leq 0.05$) were selected. The differential metabolites changes among control, model and drug experimental groups were shown in Figure 4G, 4H, 4I, heat maps.

Identification of these metabolites were carried out based on information of MS/MS and online database. A total of 88 metabolites were found to be the most significantly altered in model group relative to control group. FA and FB reversed 14, 35 of these metabolites, respectively. As listed in table 1, 36 metabolic biomarkers

involved in $CuSO_4$-induced zebrafish inflammation in FA or FB treatment groups were identified. Both FA and FB could reverse abnormal expressions of Uridine 5-Diphosphate, Carnitine, Val-Abu-OH, Ciliatine, Cytidine, Benzaldehyde, Isobutyryl Carnitine, N-Acetyl-L-Phenylalanine, Gamma-Glutamyl-Leucine, Dihydrojasmonic acid, Cyclic GMP, 12-Hydroxydodecanoic acid and N-Arachidonoyl Dihydroxypropylamine, which suggest that FA and FB may exert anti-inflammatory effect through regulating expressions of these metabolites.

Analysis of topology and pathway enrichment based on KEGG database were performed to identify the metabolomic pathways affected by these metabolites. MetaboAnalyst 4.0 was carried out to calculate the −log(p) value and the pathway impact value from analysis of pathway enrichment and topology, respectively. Potential pathways of FA and FB in $CuSO_4$-induced zebrafish inflammation were finally identified according to pathway impact and −log(p) value as summarized in Table S2. The identified biomarkers and related pathways from KEGG database were shown in Figure 4J, which indicated that the Nicotinate and nicotinamide metabolism, Energy metabolism, Pyrimidine metabolism and Purine metabolism were mainly involved.

3.5 Identification and analysis of differentially expressed proteins

The proteomic profile of $CuSO_4$-induced zebrafish after FA and FB treatment was analyzed by UPLC-MS/MS. As a result, 5212 proteins were detected. Among which, 2976 proteins were further identified and quantified with at least two unique peptides and false discovery rate (FDR) < 1%. According to the criteria of fold changes >1.5 or < 0.67 and p-values < 0.05. 146 proteins were differentially expressed in model group compared with control group, including 60 upregulated proteins and 86 downregulated proteins. Additionally, 51 and 18 differentially expressed proteins (DEPs) were reversed in the FA and FB group, respectively (Table 2).

The heat maps were presented in Figure 5A, 5B, 5C. The DEPs were categorized according to the following Gene Ontology (GO) classes: biological process, molecular function, and cellular components (Figure 5D, 5E, 5F). Compared with control group, 146 proteins were differentially expressed in model group. As for the biological processes class, the DEPs were mainly participated in binding (GO:0005488), catalytic activity (GO:0003824) and structural molecule activity (GO:0005198). In the cellular function group, the DEPs were found to be involved in cell (GO:0005623), cell part (GO:0044464) and organelle (GO:0043226). In the molecular components class, the DEPs were mainly participated in cellular process (GO:0009987), metabolic process (GO:0008152) and biological regulation (GO:0065007).

3.6 Analysis of Protein-Protein Interaction

The identified DEPs were imported to STRING for protein-protein interaction (PPI) network constructions (Figure 5G, 5H, 5I). Taking Figure 5G as an example, compared with control group, of the146 identified DEPs in model group, 101 proteins were involved in the network, 40 proteins were related to each other, and 5 proteins did not display any linkage at a confidence level of string score = 0.4. This network reflects a complex functional relationship among the proteins identified in the current study.

3.7 Interactive network of identified metabolites and proteins

The differentially expressed metabolites and proteins from groups of control vs. model, model vs. FA and model vs. FB were imported into Cytoscape software to review the significant network analyses (Figure 6A, 6B,

6C). Integrated analyses of metabolomic and proteomic studies showed altered pathways in $CuSO_4$-induced acute inflammation involving Lipid metabolism, Amino acid metabolism and Energy metabolism etc. FA and FB could reverse expressions of metabolites and proteins related to these metabolic pathways, so as to alleviate hair cells injury in zebrafish.

3.8 Gene expression in $CuSO_4$-induced zebrafish and the treatment groups

The mRNA levels of Wdr3, Nme3, Collagen, Mrps7, inflammatory mediators and genes involving in NF-κB, MAPK, JAK-STAT signaling pathways in different groups were quantified by qRT-PCR. As a result, gene expressions of Wdr3, Nme3, Collagen and Mrps7 in FA and FB treated group were decreased relative to model group, which is consistent with proteomic results (Figure 7A). Moreover, FA and FB treatment significantly downregulated IL-6, IL-1β and TNF-α expression compared with the model group (Figure 7B). FB could reverse mRNA expression of genes involving in NF-κB, MAPK and JAK3 signaling pathways. However, FA mainly exert anti-inflammation effect via NF-κB and MAPK signaling pathways (Figure 7C).

4. Discussion

FA and FB, phenylethanoid products isolated from air-dried fruits of Forsythia suspensa, have been reported to show significant effect against inflammation. Presently, the anti-inflammatory effects of FA and FB in $CuSO_4$-induced zebrafish inflammation were investigated by integrated analyses of metabolomic and proteomic. Our results showed that both FA and FB significantly inhibited $CuSO_4$-induced hair cells injury in neuromasts of zebrafish. Metabolomic and proteomic analyses indicated that FA and FB share similar anti-inflammation mechanism in some extent because of the same maternal nucleus structure. The different substituents of hydroxyl groups of FA and FB show a minor difference on the anti-inflammatory effect.

Inflammatory response is a common biological process in the body. It is highly regulated and allows the immune system to clear harmful irritants and effectively initiate reparation [17]. In the process of inflammation, excessive recruitment and uncontrolled migration of neutrophils at neuromasts could result in tissue damage and disease [16]. In this case, we used $CuSO_4$ to induced zebrafish inflammation for attractive signals of zebrafish in the whole inflammatory process can be observed, as well as monitoring the behavior of neutrophil cells during the critical transitions. Copper is a chemical metal that induces neuromasts damage of zebrafish lateral line system and can easily reflect the characteristics of antioxidant and pro-inflammatory. In addition to regenerative capacity, hair cells in zebrafish lateral line and mammal have great similarities in structure, function and molecularity [18]. In the present study, we used $CuSO_4$ to establish a chemically induced neuromasts damage inflammation model in zebrafish. Neutrophils were significantly accumulated in the damaged neuromasts of zebrafish lateral line. However, the number of neutrophils was clearly reduced when zebrafish were treated with FA or FB, which indicated the excellent therapeutic effects of FA and FB.

Excessive ROS and NO production in the body may lead to damage of cell and tissue. Hence, inhibiting the excessive production of NO and ROS can effectively inhibit the progress of inflammatory response. It can also be considered as a potential anti-inflammatory drug development strategy. Adding of $CuSO_4$ significantly increased ROS and NO production in zebrafish. However, FA and FB pre-treatment markedly inhibit ROS and NO accumulation in $CuSO_4$-induced inflammation.

Metabolomics pathway enrichment analysis indicated that the Nicotinate and nicotinamide metabolism, Energy metabolism, Pyrimidine metabolism and Purine metabolism were mainly involved, most of which are directly or partly involved in inflammation.

Nicotinamide Ribotide, also known as nicotinamide single nucleotide (NMN), can be converted into the principal precursor of nicotinamide adenine dinucleotide (NAD^+) via transamination, which is called nicotinamide [19, 20]. NAD^+ may regulate NAD^+/NADH ratio to activate SIRT1, which in turn positively regulate NF-κB expression. NF-κB is an important transcription factor and involved in pro-inflammatory cytokines generation [21, 22]. Presently, we can conclude that FB can inhibit Nicotinamide Ribotide expression so as to decrease NAD^+ synthesis, which result in an inactivation of SIRT1. Thus, NF-κB signaling pathway is suppressed and leads to a decreased release of inflammatory factors. Cytidine, Cytosine, Deoxyuridine, Uracil, XMP, dIMP, Cyclic GMP and Guanosine, which are all involved in the Pyrimidine and Purine metabolism that participated in 14 different diseases development processes and representing a wide range of clinical manifestations [23]. It has become clear that pyrimidines and purines are important in cellular immunodeficiency and infections. Hence, we can conclude that FA and FB might regulate metabolites to reverse cellular immunodeficiency and recurrent infections to exert anti-inflammation effect.

At the same time, energy consumption also plays an important role during the development of inflammation. In the present study, Starch and sucrose metabolism, Amino sugar and nucleotide sugar metabolism, Glycolysis, Pentose phosphate pathway (PPP) and Galactose metabolism are all related to energy metabolism. Glucose-6-phosphate (G6P) is the intersection of multiple metabolic pathways that can be converted to PPP for NADPH and ribose-5-phosphate. Activation of PPP leads to an inhibition of P53, which increases glucose consumption, NADPH production and biosynthesis [24]. That is, in $CuSO_4$-induced acute inflammation, zebrafish need more energy to repair itself. In our study, G6P was upregulated significantly in model group versus control group, but FB downregulated G6P remarkably, suggesting that FB sever as an anti-inflammatory agent though regulating energy metabolism and restoration of balance.

The DEPs identified by proteomics analyses are primarily involved in cellular process and functions, metabolic process and biological regulation. Previous studies have shown that the organization of ROS, NF-κB and collagen at the injury margin are involved in promotion of wound healing [25]. In addition to the generation of collagen, remodeling of the collagen structure induced by tissue damage also plays a key step in the repair process, which may be achieved by the proteases action such as matrix metalloproteinase (MMP) [26, 27]. The important role of MMP9 in collagen reorganization and regeneration after zebrafish tail transection have also been reported [28]. Our findings suggest that both FA and FB could reverse collagen organization, guiding therapeutics focused on optimal repair of chemically induced hair cells wounds in zebrafish larvae. NME, also known as NM-23, participates in a variety of physiological and pathological cellular processes such as differentiation, development, cellular signaling and cellular function. It has been reported that Nm23-H1 could interacts with p53 and positively regulates apoptosis and arrest of cell cycle induced by p53 [29]. In the present study, both FA and FB could downregulate NME3 expression, which indicate a potential regulation of cell signaling and functions of FA and FB.

Mitochondrial ribosomal protein (MRP) subunits are nuclear-encoded [30], some of which are reported to be involved in mitochondrial diseases. MRPS22 and MRPS16 are protein subunits encoded by small 28S subunit

and have been reported to cause a combined respiratory chain enzyme deficiency [31]. MRPS7, a 12S ribosomal RNA binding subunit, which is necessary for assembly of small ribosomal subunits. Studies have confirmed that MRPS7 mutations can cause mitochondrial respiratory chain dysfunction and congenital sensorineural deafness [32]. As a member of the WDR repeat proteins, WDR3 participates in several cellular processes such as cell cycle progression and signal transduction [33, 34]. Studies have confirmed that some WDR-repeat proteins are participated in the transduction of MAPK and STAT3 signaling pathways [35]. Here we can speculate that FA and FB might reverse the expression of MRPS7 and WDR3 proteins to regulate mitochondrial function, cell cycle progression and signal pathways transduction.

As a summary, we produced a brief FA and FB action diagram (Fig. 8). FA and FB can inhibit ROS and NO production, down-regulate expressions of WDR3, Collagen, NME3 and MRPS7, and reverse the secretion of inflammatory mediators induced by $CuSO_4$, thus prevent inflammation cascade reaction.

5. Conclusion

In conclusion, we analyzed the inhibitory effect and therapeutic mechanism of FA and FB in $CuSO_4$-induced zebrafish inflammation using UPLC-MS/MS based metabolomics and TMT-6 Plex based proteomics for the first time. A series of metabolic intermediates and proteins were altered during the development of inflammation. These biomarkers may clarify the anti-inflammatory mechanism of FA and FB in chemically induced zebrafish acute inflammation. These findings indicated a potential novel and sequential mechanism for the initiation of $CuSO_4$-induced zebrafish inflammation and highlighted the potential therapeutic effect of FA and FB.

Declarations

Additional file

Additional file 1: Table S1. Table S1: Primers used for quantitative real-time PCR.

Additional file 2: Table S2. Metabolic pathways associated to varied influences of FA and FB in $CuSO_4$-induced zebrafish inflammation.

Ethics approval and consent to participate

All experiments were performed consistent with animal use in science in European Communities Council Directive (2010/63/EU) and followed by Chengdu University of Traditional Chinese Medficine of Laboratory Animal Ethics Committee.

Consent for publication

Not applicable.

Availability of data and materials

The datasets generated and/or analyzed in the current study are available from the corresponding author on reasonable request.

Competing interests

The authors declare no conflicts of interest.

Funding

The study was supported by National Natural Science Foundation of China (No:81373943, 81573583), Sichuan Provincial Science and Technology Department of Youth Science and technology innovation research team program (2016TD0006, 2017TD0001).

Author contributions

L.G. and Y.L. conceived and designed the experiments. L.G., L.Y., X.G., C.W., N.H. and X.D conducted the biological experiments and analyzed the data. L.G. and Y.L. wrote the manuscript. All the authors read and approved the final manuscript.

Acknowledgements

We thank Dr. Mei-chen Liu for her critical revision of the manuscript for important metabolic pathway analysis content.

Studies involving human participants, human data, or human tissue

Not applicable.

Abbreviations

FA, Forsythiaside A; FB, Forsythiaside B; dpf, day post-fertilization; DCF-DA, 2,7-dichlorodihydrofluorescein diacetate; DAF-FMDA, diamino fluorophore 4-amino-5-methylamino-2',7'-difluorofluorescein diacetate; PCA, principal component analysis; PLS-DA, partial least squares-discriminant analysis; OPLS-DA, orthogonal projections to latent structures discriminant analysis; BPC, Base Peak Chromatogram; DEPs, differentially expressed proteins; FDR, false discovery rate; GO, Gene Ontology; PPI, Protein-Protein Interaction; NMNM, nicotinamide single nucleotide; NAD+, nicotinamide adenine dinucleotide; PPP, Pentose phosphate pathway; MRP, Mitochondrial ribosomal protein.

References

[1] Bhattacharya K, Andón FT, El-Sayed R, Fadeel B. Mechanisms of carbon nanotube-induced toxicity: focus on pulmonary inflammation. Adv Drug Deliver Rev. 2013;65(15):2087-2097.

[2] Freire MO, Van Dyke TE. Natural resolution of inflammation. Periodontol 2000. 2013;63(1):149-164.

[3] Muralidharan S, Mandrekar P. Cellular stress response and innate immune signaling: integrating pathways in host defense and inflammation. J Leukocyte Biol. 2013;94(6):1167-1184.

[4] Chen HY, Lin YH, Huang JW, Chen YC. Chinese herbal medicine network and core treatments for allergic skin diseases: implications from a nationwide database. J Ethnopharmacol. 2015;168:260-267.

[5] Pan CW, Zhou GY, Chen WL. Protective effect of forsythiaside a on lipopolysaccharide/d-galactosamine-induced liver injury. Int Immunopharmacol. 2015;26(1):80-85.

[6] Jiang WL, Fu FH, Xu BM, Tian JW, Zhu HB, Jian-Hou. Cardioprotection with forsythoside b in rat myocardial ischemia-reperfusion injury: relation to inflammation response. Phytomedicine. 2010;17(8-9):635-639.

[7] Lee SH, Ko CI, Jee Y, Jeong Y, Jeon YJ. Anti-inflammatory effect of fucoidan extracted from ecklonia cava in zebrafish model. Carbohyd Polym. 2013;92(1):84-89.

[8] Meeker ND, Trede NS. Immunology and zebrafish: spawning new models of human disease. Dev Comp Immunol. 2008;32(7):0-757.

[9] Nusslein VC, Dahm R (eds). Zebrafish: A Practical Approach. Oxford University Press. 2002; Oxford, UK.

[10] Yang Y, Zheng K, Mei W, Wang Y, Hu J. Anti-inflammatory and proresolution activities of bergapten isolated from the roots of ficus hirta in an in vivo zebrafish model. Biochemical and Biophysical Research Communications. 2018;496(2):763-769.

[11] Unwin RD, Griffiths JR, Whetton AD. Simultaneous analysis of relative protein expression levels across multiple samples using itraq isobaric tags with 2d nano lc–ms/ms. Nat Protoc. 2010;5(9):1574-1582.

[12] Crowell AM, Wall MJ, Doucette AA. Maximizing recovery of water-soluble proteins through acetone precipitation. Anal Chim Acta. 2013;796:48-54.

[13] Käll L, Canterbury JD, Weston J, Noble WS, Maccoss MJ. Semi-supervised learning for peptide identification from shotgun proteomics datasets. Nat Methods. 2007;4(11):923-925.

[14] Olivari FA, Hernández PP, Allende ML. Acute copper exposure induces oxidative stress and cell death in lateral line hair cells of zebrafish larvae. Brain Res. 2008;1244:1-12.

[15] Mills EL, O'Neill LA. Reprogramming mitochondrial metabolism in macrophages as an anti-inflammatory signal. Eur J Immunol. 2016;46(1):13-21.

[16] Tripathi P, Tripathi P, Kashyap L, Singh V. The role of nitric oxide in inflammatory reactions. Fems Immunol Med Mic. 2007;51(3):443-452.

[17] Gernez Y, Tirouvanziam R, Chanez P. Neutrophils in chronic inflammatory airway diseases: can we target them and how? Eur Respir J. 2010;35(3):467-469.

[18] Christine DC, Dora S, Fabien S, Kelly D, Nicolas G, Alain G. The lateral line of zebrafish: a model system for the analysis of morphogenesis and neural development in vertebrates. Biol Cell. 2003;95(9):579-587.

[19] Penberthy WT. Editorial [hot topic: nicotinamide adenine dinucleotide biology and disease (executive editor: w. todd penberthy)]. Curr Pharm Design. 2009;15(1):1-2.

[20] Zhai RG, Rizzi M, Garavaglia S. Nicotinamide/nicotinic acid mononucleotide adenylyltransferase, new insights into an ancient enzyme. Cell Mol Life Sci. 2009;66(17):2805-2818.

[21] Matsushita T, Sasaki H, Takayama K, Ishida K, Kuroda R. The overexpression of sirt1 inhibited osteoarthritic gene expression changes induced by interleukin-1 in human chondrocytes. J Orthop Res. 2013;31(4):531-537.

[22] Imai SI. The nad world: a new systemic regulatory network for metabolism and aging—sirt1, systemic nad biosynthesis, and their importance. Cell Biochem Biophys. 2009;53(2):65-74.

[23] Nyhan WL. Disorders of purine and pyrimidine metabolism. Mol Genet Metab. 2005;86(1-2):0-33.

[24] Jiang P, Du W, Wang X, Mancuso A, Gao X, Wu M, Yang X. P53 regulates biosynthesis through direct inactivation of glucose-6-phosphate dehydrogenase. Nat Cell Biol. 2011;13(3):310-316.

[25] LeBert D, Squirrell JM, Freisinger C, Rindy J, Golenberg N, Frecentese G, Gibson A, Eliceiri KW, Huttenlocher A. Damage-induced reactive oxygen species regulate vimentin and dynamic collagen-based projections to mediate wound repair. Elife. 2018;7:e30703.

[26] Cheng F, Shen Y, Mohanasundaram P, Lindström M, Ivaska J, Ny T, Eriksson JE. Vimentin coordinates fibroblast proliferation and keratinocyte differentiation in wound healing via tgf-β–slug signaling. Proc Natl Acad Sci USA. 2016;113(30):E4320-E4327.

[27] Eckes B, Colucciguyon E, Smola H, Nodder S, Babinet C, Krieg T, Martin P. Impaired wound healing in embryonic and adult mice lacking vimentin. J Cell Sci. 2000;113(13):2455-2462.

[28] Lebert DC, Squirrell JM, Rindy J, Broadbridge E, Lui Y, Zakrzewska A, Eliceiri KW, Meijer AH, Huttenlocher A. Matrix metalloproteinase 9 modulates collagen matrices and wound repair. Development. 2015;142(12):2136-2146.

[29] Boissan M, Dabernat S, Peuchant E, Schlattner U, Lascu I, Lacombe ML. The mammalian nm23/ndpk family: from metastasis control to cilia movement. Mol Cell Biochem. 2009;329(1-2):51-62.

[30] Brodersen DE, Nissen P. The social life of ribosomal proteins. FEBS J. 2005;272(9):2098-2108.

[31] Smits P, Saada A, Wortmann SB, Heister AJ, Brink M, Pfundt R, Miller C, Haas D, Hantschmann R, Rodenburg RJ, Smeitink JA, van den Heuvel LP. Mutation in mitochondrial ribosomal protein mrps22 leads to cornelia de lange-like phenotype, brain abnormalities and hypertrophic cardiomyopathy. Eur J Hum Genet. 2010;19(4):394-399.

[32] Menezes MJ, Guo Y, Zhang J, Riley LG, Cooper ST, Thorburn DR, Li J, Dong D, Li Z, Glessner J, Davis RL, Sue CM, Alexander SI, Arbuckle S, Kirwan P, Keating BJ, Xu X, Hakonarson H, Christodoulou J. Mutation in mitochondrial ribosomal protein s7 (mrps7) causes congenital sensorineural deafness, progressive hepatic and renal failure and lactic acidemia. Hum Mol Genet. 2015;24(8):2297-2307.

[33] Van der Voorn L, Ploegh HL. The wd-40 repeat. Febs Lett. 1992; 307(2): 131-134.

[34] Smith TF, Gaitatzes C, Saxena K, Never EJ. The wd repeat: a common architecture for diverse functions. Trends Biochem Sci. 1999;24(5):181.

[35] Zhu Y, Wang Y, Xia C, Li D, Li Y, Zeng W, Yuan W, Liu H, Zhu C, Wu X, Liu M. Wdr26: a novel gβ-like protein, suppresses mapk signaling pathway. J Cell Biochem. 2004;93(3):579–587.

Tables

Table 1. Identification results and change trends of important differential metabolites

No.	Metabolities	m/z	Rt/s	ESI mode	Formula	VIP	P-value	Control vs Model	Model vs FA	Model vs FB
1	Uridine 5-Diphosphate	402.99	71.91	−	$C_9H_{14}N_2O_{12}P_2$	1.793	0.001	↑###	↓**	↓***
2	XMP	363.03	75.89	−	$C_{10}H_{13}N_4O_9P$	2.133	0.000	↑###	−	↓***
3	Pipecolic acid	130.08	78.20	+	$C_6H_{11}NO_2$	1.242	0.034	↑#	−	↓*
4	Carnitine	162.11	91.92	+	$C_7H_{16}NO_3$	1.288	0.027	↑#	↓*	↓*
5	5-Methoxyindoleacetate	206.08	97.77	+	$C_{11}H_{11}NO_3$	1.728	0.001	↑##	−	↓*
6	Cytosine	112.05	101.80	+	$C_4H_5N_3O$	1.295	0.026	↑#	−	↓*
7	Nicotinamide Ribotide	335.06	102.13	+	$C_{11}H_{15}N_2O_8P$	1.990	0.000	↑###	−	↓***
8	Trigonelline	138.05	102.30	+	$C_7H_7NO_2$	1.592	0.004	↑##	−	↓*
9	1-Aminocyclohexanecarboxylic acid	144.10	102.86	+	$C_7H_{13}NO_2$	1.787	0.001	↑###	−	↓*
10	N-Alpha-Acetyllysine	189.12	104.90	+	$C_8H_{16}N_2O_3$	1.275	0.028	↑#	−	↓*
11	Val-Abu-OH	309.11	105.87	−	$C_{14}H_{18}N_2O_6$	1.655	0.003	↑##	↓*	↓**
12	Chitobiose	425.17	107.48	+	$C_{16}H_{28}N_2O_{11}$	1.940	0.000	↑###	↓**	-
13	Glutamylthreonine	249.11	110.44	+	$C_9H_{16}N_2O_6$	1.477	0.009	↑##	−	↓***
14	Glucose 6-Phosphate	261.03	112.61	+	$C_6H_{13}O_9P$	1.458	0.000	↑#	−	↓***
15	dIMP	331.04	115.74	−	$C_{10}H_{13}N_4O_7P$	1.280	0.029	↓#	−	↑**
16	Ciliatine	126.03	118.96	+	$C_2H_8NO_3P$	1.180	0.000	↑###	↓***	↓***
17	N6-Acetyl-L-Lysine	189.12	121.39	+	$C_8H_{16}N_2O_3$	1.193	0.042	↑#	−	↓*
18	N-A-Acetyl-L-Arginine	217.13	121.98	+	$C_8H_{16}N_4O_3$	1.751	0.001	↑##	−	↓**
19	Uracil	113.03	139.01	+	$C_4H_4N_2O_2$	1.645	0.003	↓##	−	↑*
20	Cytidine	242.08	174.43	−	$C_9H_{13}N_3O_5$	1.464	0.011	↑#	↓*	↓**
21	Guanosine	282.08	230.23	−	$C_{10}H_{13}N_5O_5$	1.399	0.015	↑#	−	↓***

22	Deoxyuridine	227.06	289.06	−	$C_9H_{12}N_2O_5$	1.363	0.019	↓#	−	↑*
23	L-Beta-Homomethionine	164.07	336.67	+	$C_6H_{13}NO_2S$	1.215	0.038	↑#	−	↓**
24	Gamma-Glutamyl-Methionine	279.10	337.22	+	$C_{10}H_{19}N_3O_4S$	2.147	0.000	↑###	−	↓***
25	Benzaldehyde	107.05	343.55	+	C_7H_6O	1.794	0.001	↑##	↓**	↓**
26	Isobutyryl Carnitine	232.15	373.56	+	$C_{11}H_{21}NO_4$	1.208	0.040	↑#	↓*	↓*
27	N-Acetyl-L-Phenylalanine	206.08	385.01	−	$C_{11}H_{13}NO_3$	1.590	0.005	↑##	↓*	↓**
28	Gamma-Glutamyl-Leucine	261.14	404.26	+	$C_{11}H_{21}N_3O_4$	1.904	0.000	↑###	↓**	↓**
29	Jasmonate	209.12	521.42	−	$C_{12}H_{18}O_3$	1.045	0.000	↓##	−	↑***
30	N-Acetyltryptophan	247.11	543.58	+	$C_{13}H_{14}N_2O_3$	1.478	0.010	↑##	−	↓**
31	Dihydrojasmonic acid	211.13	601.25	−	$C_{12}H_{20}O_3$	1.348	0.020	↓#	↑*	↑**
32	Cyclic GMP	344.07	625.18	−	$C_{10}H_{12}N_5O_7P$	1.731	0.002	↓##	↑***	↑**
33	12-Hydroxydodecanoic acid	215.16	710.07	−	$C_{12}H_{24}O_3$	1.780	0.001	↑##	↓*	↓*
34	NAGly	360.25	794.64	−	$C_{22}H_{35}NO_3$	2.005	0.000	↑###	−	↓**
35	L-A-Lysophosphatidylserine	524.30	823.98	−	$C_{24}H_{48}NO_9P$	1.246	0.034	↓#	−	↑**
36	N-Arachidonoyl Dihydroxypropylamine	376.29	825.78	−	$C_{23}H_{39}NO_3$	1.643	0.003	↓##	↑**	↑**

↑represent upregulated; ↓ represent downregulated.

# $P < 0.05$, ## $P < 0.01$, ### $P < 0.001$, compared with control group.

* $P < 0.05$, ** $P < 0.01$, *** $P < 0.001$, compared with model group.

Table 2. Dysregulated Proteins in different groups

No.	Accession	Gene Symbol	Description	Control vs Model	Model vs FA	Model vs FB
1	NP_001014348	srpx	sushi repeat-containing protein SRPX precursor	↓##	↑**	↑*
2	NP_001028768	mrps7	28S ribosomal protein S7, mitochondrial precursor	↑###	↓***	↓***
3	NP_001077285	zgc:162509	uncharacterized protein LOC553299	↑##	↓**	↓**
4	NP_001268407	col2a1b	collagen, type II, alpha 1b precursor	↑##	↓**	↓***
5	NP_571742	gch2	GTP cyclohydrolase 1	↑##	↓***	↓**
6	NP_942574	wdr3	WD repeat-containing protein 3	↑##	↓*	↓*
7	NP_956140	ptpn11a	tyrosine-protein phosphatase non-receptor type 11	↑#	↓*	↓*
8	NP_956258	rcvrn2	recoverin 2	↓#	↑**	↑**
9	NP_991174	nit2	omega-amidase NIT2	↑#	↓*	↓*
10	NP_997744	col9a2	collagen alpha-2(IX) chain precursor	↓##	↑***	↑***
11	NP_998429	col9a1b	collagen type IX alpha I precursor	↑##	↓**	↓***
12	XP_021324964	nme3	nucleoside diphosphate kinase 3 isoform X1	↑###	↓***	↓***
13	XP_695887	scaf4a	splicing factor, arginine/serine-rich 15	↓#	↑*	↑**
14	NP_001002461	txn	thioredoxin	↓##	↑*	-
15	NP_001003625	nup85	nuclear pore complex protein Nup85	↑#	↓**	-
16	NP_001004660	snrpg	small nuclear ribonucleoprotein G isoform 2	↓#	↑*	-
17	NP_001006043	ctsz	cathepsin Z precursor	↓#	↑*	-
18	NP_001017899	capns1a	calpain small subunit 1	↓#	↑**	-
19	NP_001019906	eif3m	eukaryotic translation initiation factor 3 subunit M	↓##	↑**	-
20	NP_001020680	ppp6r2a	serine/threonine-protein phosphatase 6 regulatory subunit 2	↑##	↓**	-
21	NP_001038800	rpl22l1	60S ribosomal protein L22-like 1	↓###	↑***	-

22	NP_001071203	bop1	ribosome biogenesis protein bop1	↑#	↓**	-
23	NP_001082840	mrps30	39S ribosomal protein S30, mitochondrial	↓#	↑*	-
24	NP_001093210	matn1	cartilage matrix protein precursor	↓#	↑***	-
25	NP_001096604	crygm2d16	crystallin, gamma M2d16	↓##	↑***	-
26	NP_001103591	rps23	40S ribosomal protein S23	↓#	↑*	-
27	NP_001166027	bxdc2	ribosome biogenesis protein BRX1 homolog	↑##	↓**	-
28	NP_001289671	atp5f1e	ATP synthase subunit epsilon, mitochondrial	↓##	↑**	-
29	NP_001338629	LOC100330864	ribonucleoside-diphosphate reductase subunit M2 isoform 1	↑#	↓*	-
30	NP_571328	opn1mw1	green-sensitive opsin-1	↓##	↑*	-
31	NP_956159	cdc42l	cell division control protein 42 homolog	↓#	↑*	-
32	NP_956500	erap1b	endoplasmic reticulum aminopeptidase 1 precursor	↓#	↑*	-
33	NP_957036	rps26l	ribosomal protein S26	↓#	↑**	-
34	NP_957153	slc25a20	mitochondrial carnitine/acylcarnitine carrier protein	↓#	↑**	-
35	NP_958493	pfn2	profilin 2	↓##	↑*	-
36	NP_958500	arpc1a	actin-related protein 2/3 complex subunit 1A	↓#	↑**	-
37	NP_963878	rpl12	60S ribosomal protein L12	↓##	↑*	-
38	NP_991317	psmd10	26S proteasome non-ATPase regulatory subunit 10	↓#	↑*	-
39	NP_997743	mcmbp	mini-chromosome maintenance complex-binding protein	↓##	↑*	-
40	NP_997750	ist1	IST1 homolog isoform 1	↓##	↑***	-
41	NP_998569	lipf	lysosomal acid lipase/cholesteryl ester hydrolase precursor	↓#	↑*	-
42	NP_998605	plrg1	pleiotropic regulator 1	↑##	↓**	-
43	NP_999858	lgals3b	galectin-3	↓##	↑***	-

44	NP_999977	epb41l3b	erythrocyte membrane protein band 4.1-like 3b	↑#	↓*	-
45	XP_001923961	nxf1	nuclear RNA export factor 1	↑##	↓*	-
46	XP_005159500	col11a2	collagen alpha-2(XI) chain isoform X1	↓##	↑*	-
47	XP_005163206	tnni2a.4	troponin I, skeletal, fast 2a.4 isoform X1	↑##	↓***	-
48	XP_017208249	coro6	coronin-6 isoform X1	↓#	↑***	-
49	XP_021322373	arhgef1b	rho guanine nucleotide exchange factor 1 isoform X1	↓##	↑**	-
50	XP_685270	sgca	alpha-sarcoglycan	↑#	↓**	-
51	XP_691943	si:dkey-23a13.8	histone H2B 1/2-like	↑##	↓**	-
52	NP_001019612	psma2	proteasome alpha 2 subunit	↑#	-	↓*
53	NP_001071216	scg2b	secretogranin-2 precursor	↓##	-	↑**
54	NP_001313480	si:dkey-251i10.2	si:dkey-251i10.2 precursor	↓#	-	↑*
55	NP_957419	spag7	sperm-associated antigen 7 homolog	↑#	-	↓*
56	XP_005155974	si:ch211-222l21.1	prothymosin alpha	↑###	-	↓**

↑represent upregulated; ↓ represent downregulated.

# $P < 0.05$, ## $P < 0.01$, ### $P < 0.001$, compared with control group.

*$P < 0.05$, ** $P < 0.01$, ***$P < 0.001$, compared with model group.

Figures

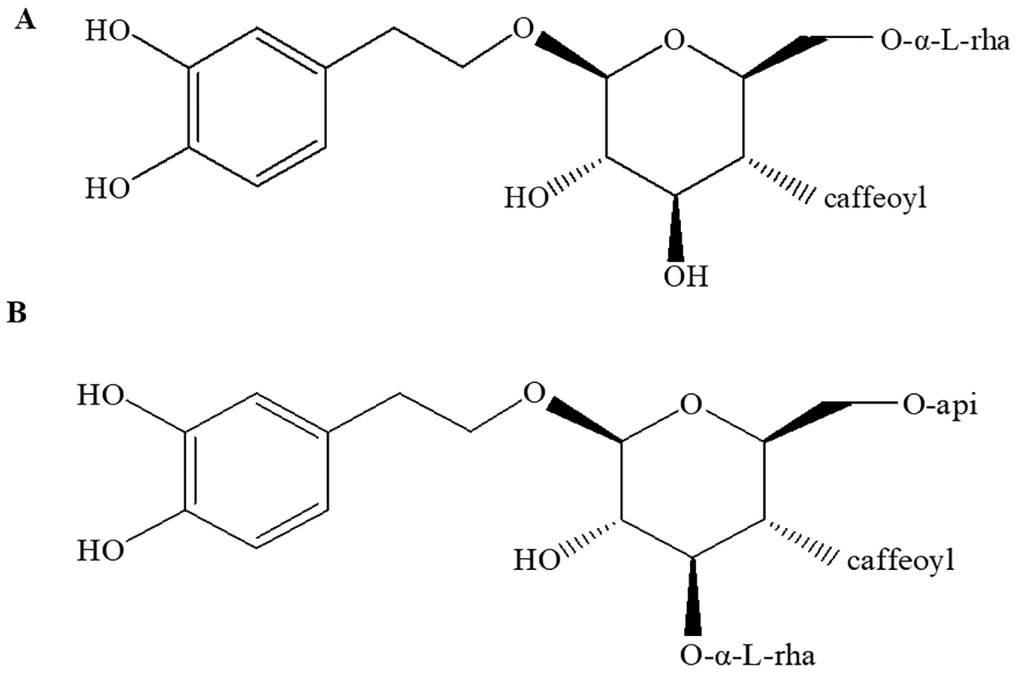

Figure 1

Chemical structures of Forsythiaside A (A) and Forsythiaside B (B).

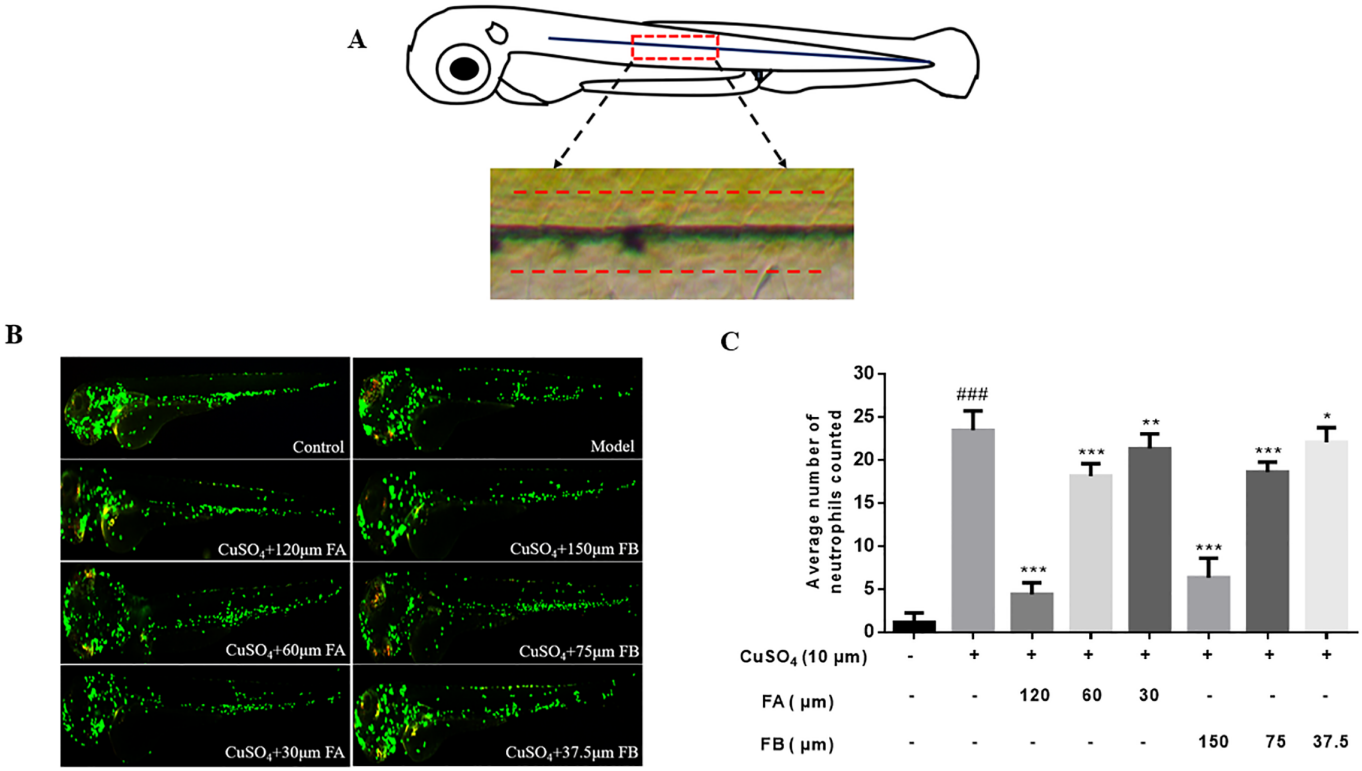

Figure 2

FA and FB inhibit neutrophils recruitment to the injury site in CuSO4 treated zebrafish. (A) A general view of a 3 dpf zebrafish larva. The boxed area refers to the horizontal lateral line, and neutrophils within the horizontal line (dotted red lines) were calculated in quantification experiments. (B) Microphotographs showing neutrophils migration in control group, model group and FA and FB treatment groups in different concentrations (neutrophils of 3 dpf transgenic (mpx:EGFP) zebrafish exhibiting green fluorescence, n=15 per group). (C) FA and FB dose-dependently reduced number of neutrophils counted in the injury site (n=15 per group). Data are shown as mean ± S.D. # P < 0.05, ## P < 0.01, ### P < 0.001, compared with control group; * P < 0.05, ** P < 0.01, *** P < 0.001, compared with model group.

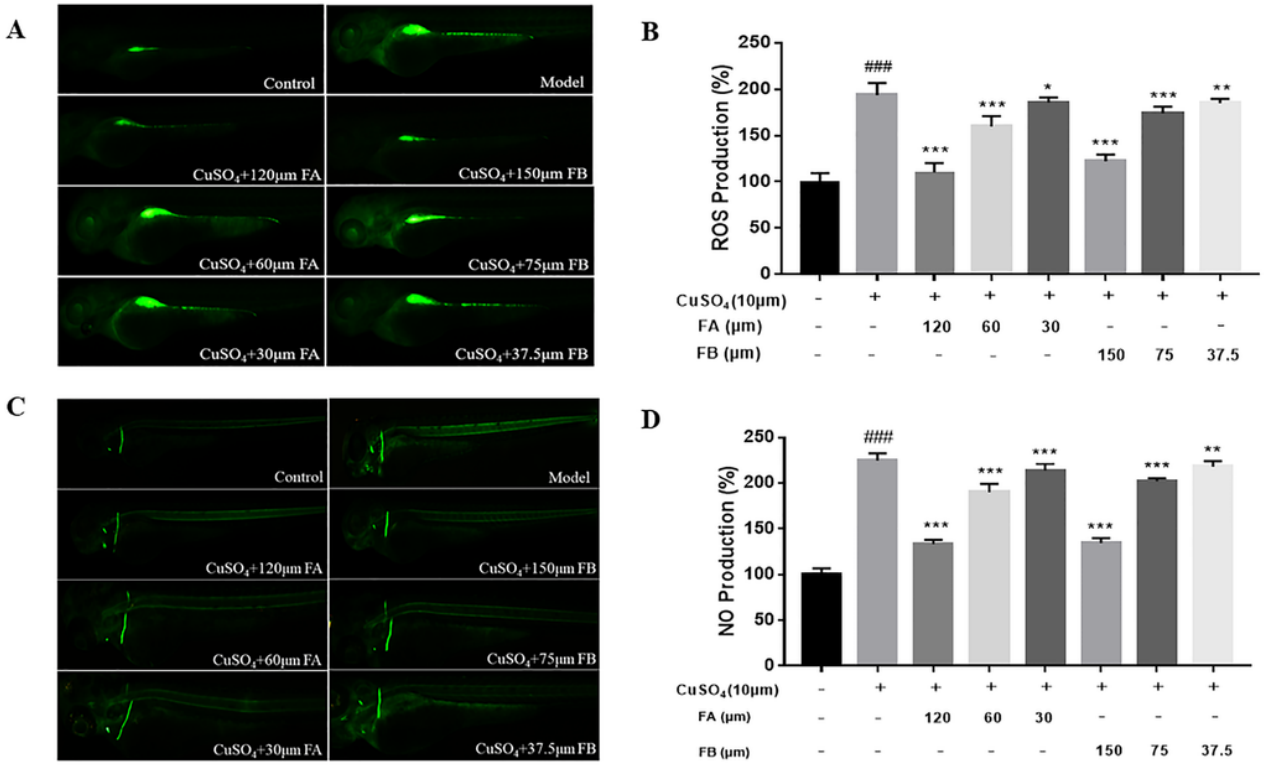

Figure 3

FA and FB alleviated zebrafish inflammation by inhibiting CuSO4-induced ROS and NO generation. (A) Microphotographs documenting ROS production in control group, model group, FA and FB treatment groups in different concentrations (3 dpf Wild-type AB zebrafish larvae). (B) FA and FB dose-dependently reduced CuSO4-induced ROS generation. (C) Microphotographs documenting production of NO in control group, model group, FA and FB treatment groups in different concentrations (3 dpf Wild-type AB zebrafish larvae). (D) FA and FB dose-dependently reduced CuSO4-induced NO generation. Data are shown as mean ± S.D, n=15 per group. # P < 0.05, ## P < 0.01, ### P < 0.001, compared with control group; * P < 0.05, ** P < 0.01, *** P < 0.001, compared with model group.

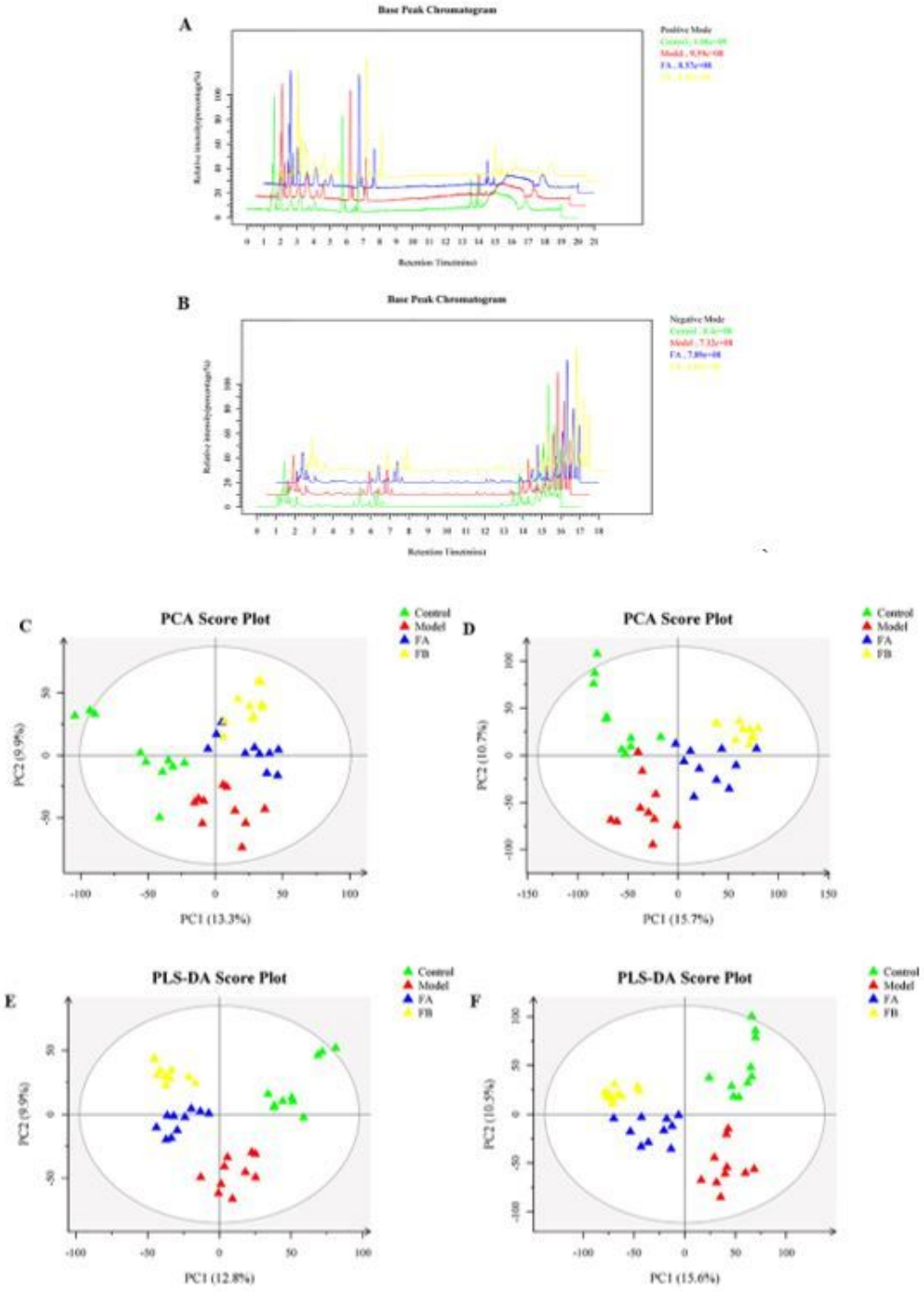

Figure 4

UPLC-MS/MS data analysis. Representative Base Peak Chromatogram (BPC) of the zebrafish in the control, model, FA, FB groups obtained from positive ion mode (A) and negative ion mode (B). PCA score plot of zebrafish metabolites from positive ion mode (C) and negative ion mode (D). PLS-DA score plot of zebrafish metabolites from positive ion mode (E) and negative ion mode (F). Heat-map of metabolites of control vs. model (G), model vs. FA (H), model vs. FB (I). Rows: metabolites; columns: zebrafish samples. The rectangle in different color represent the expression level of metabolites. Highest in red; lowest in blue; mean in white. (J) Metabolic pathways (bold) participating in the anti-inflammation action of FA and FB in CuSO4-induced

zebrafish model. The metabolites (red) are identified biomarkers in the present study. Arrows nearby metabolites indicated relative expressions in each group.

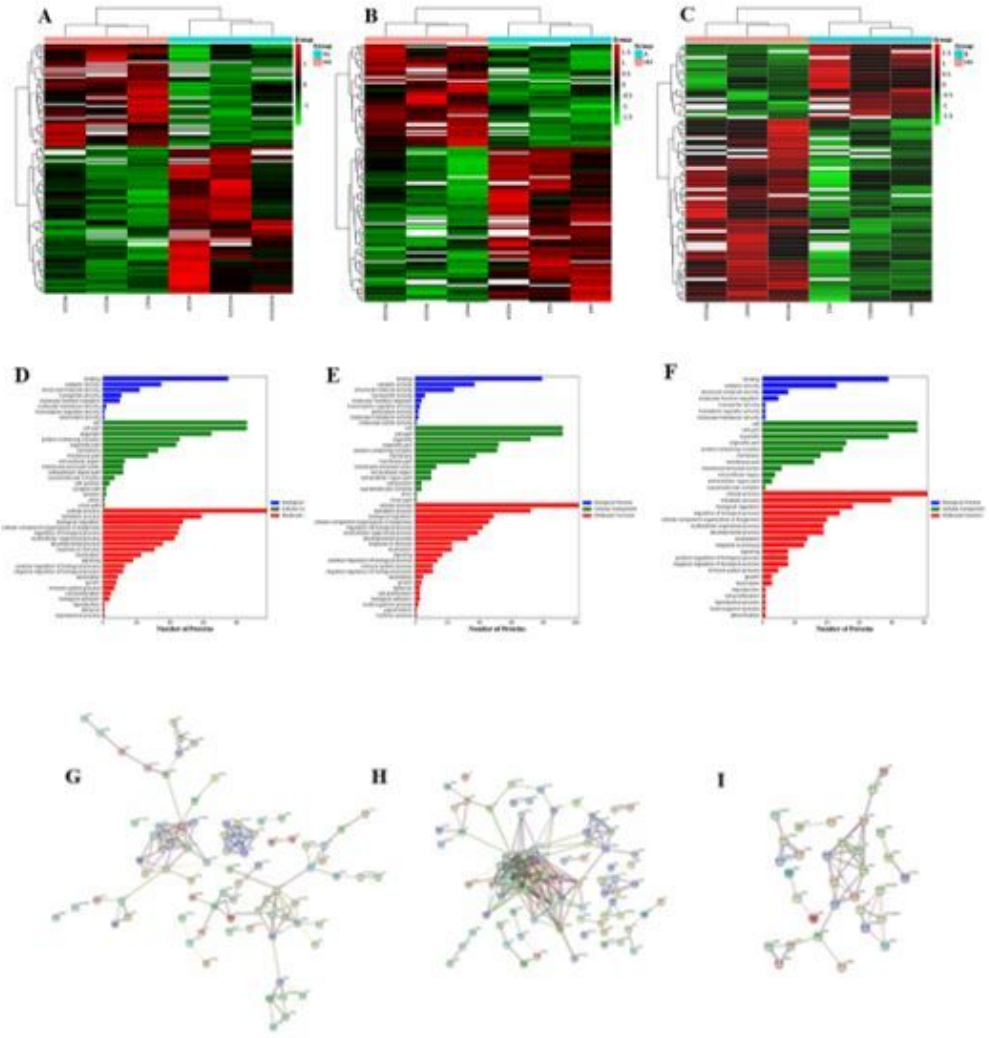

Figure 5

Proteomic analyses of zebrafish larvae. Heat-map of differential proteins of control vs. model (A), model vs. FA (B), model vs. FB (C). Rows: proteins; columns: samples. The rectangle in different color represent the expression level of proteins. Highest in red; lowest in green; mean in white. GO analysis of differential proteins of control vs. model (D), model vs. FA (E), model vs. FB (F). Rows: proteins number; Columns: GO functional classification. Protein-protein interactions of diferential proteins from control vs. model (G), model vs. FA (H), model vs. FB (I).

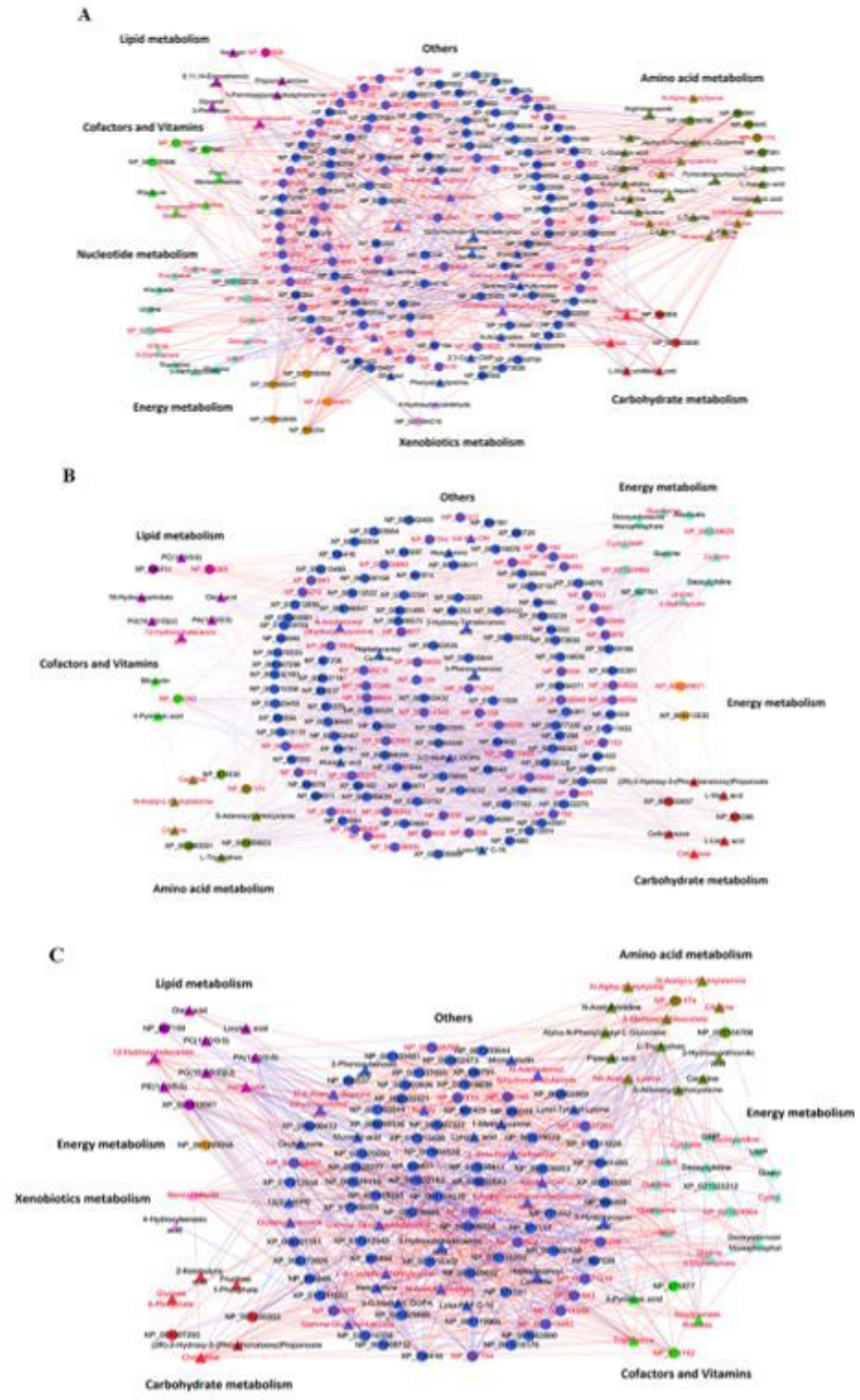

Figure 6

Interactive network construction by integrated metabolomics and proteomics analysis. Interactive network of the metabolites and proteins of model compared with control (A), FA (B), and FB (C). Triangles and circles in different colors represent metabolites and proteins in different metabolic pathways. The metabolites and proteins in red represent identified biomarkers in the present study.

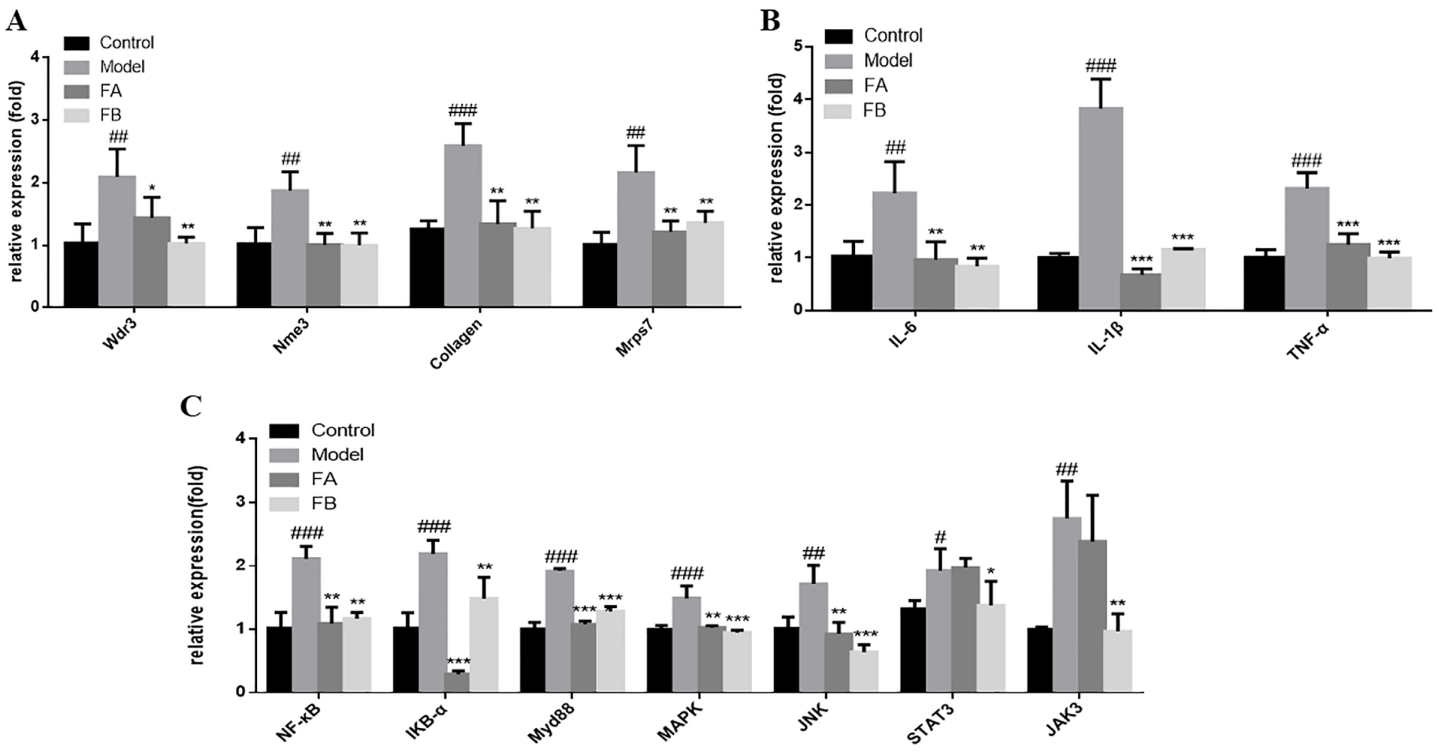

Figure 7

Relative expression of mRNA in different groups as detected by qRT-PCR. (A) The mRNA expression of Wdr3, Nme3, Collagen, Mrps7 of control, model, FA and FB groups. (B) The mRNA expression of IL-6, IL-1β, TNF-α of control, model, FA and FB groups. (C) The mRNA expression of genes involved in NF-κB, MAPK, JAK-STAT signaling pathways of control, model, FA and FB groups. Data are shown as mean ± S.D, n=35 per group. # P < 0.05, ## P < 0.01, ### P < 0.001, compared with control group; * P < 0.05, ** P < 0.01, *** P < 0.001, compared with model group.

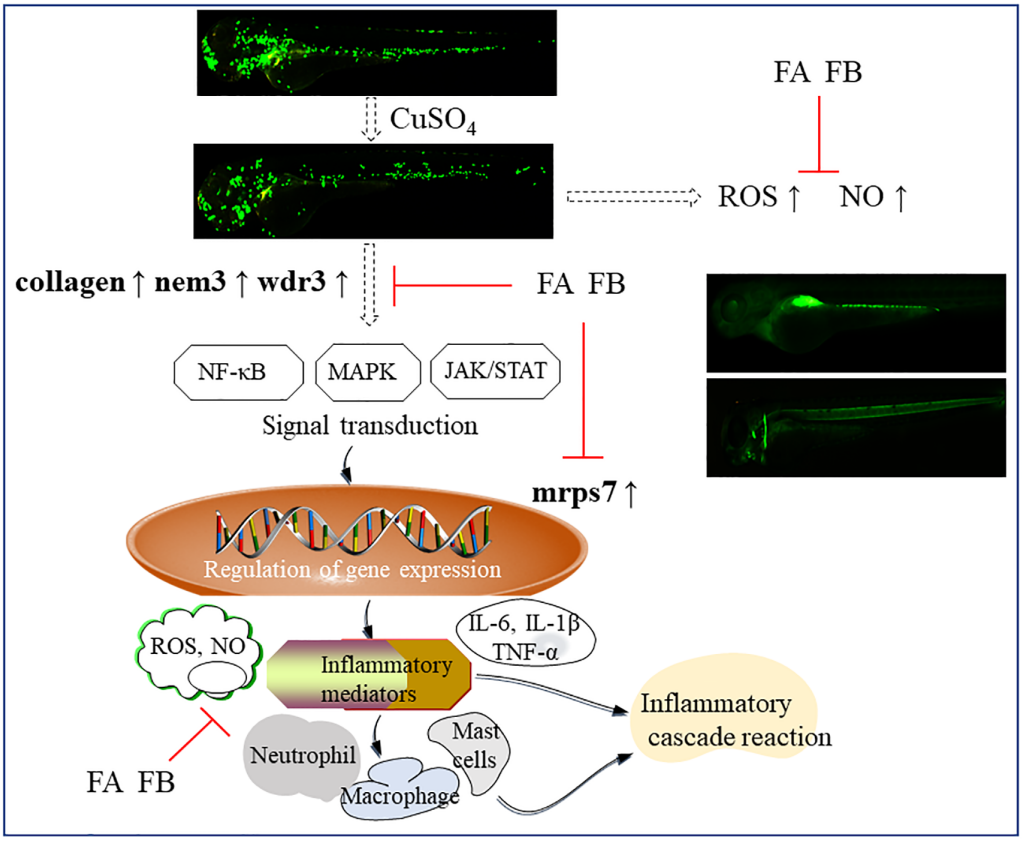

Figure 8

A probable mechanism of FA and FB in the protection of CuSO4-induced zebrafish inflammation.

Supplementary Files

This is a list of supplementary files associated with this preprint. Click to download.

- Additionalfile1.docx
- Additionalfile2.docx